

RSC Advances



This is an *Accepted Manuscript*, which has been through the Royal Society of Chemistry peer review process and has been accepted for publication.

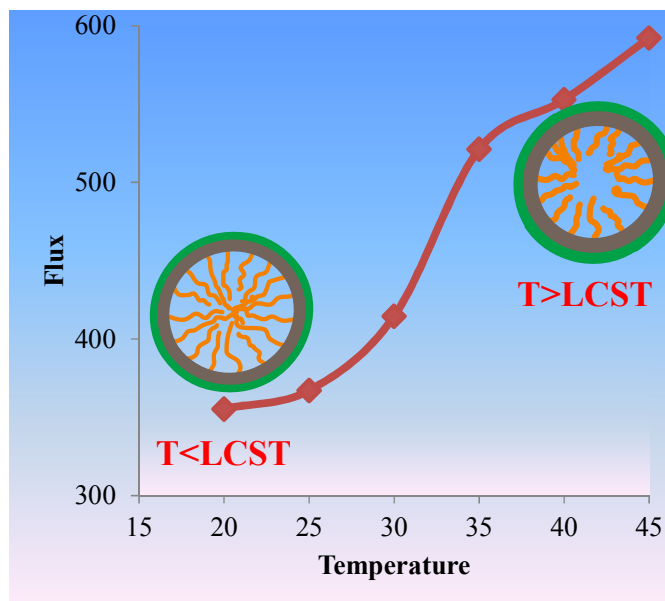
Accepted Manuscripts are published online shortly after acceptance, before technical editing, formatting and proof reading. Using this free service, authors can make their results available to the community, in citable form, before we publish the edited article. This *Accepted Manuscript* will be replaced by the edited, formatted and paginated article as soon as this is available.

You can find more information about *Accepted Manuscripts* in the [Information for Authors](#).

Please note that technical editing may introduce minor changes to the text and/or graphics, which may alter content. The journal's standard [Terms & Conditions](#) and the [Ethical guidelines](#) still apply. In no event shall the Royal Society of Chemistry be held responsible for any errors or omissions in this *Accepted Manuscript* or any consequences arising from the use of any information it contains.

Graphical Abstract

Thermoresponsive membranes with good antifouling ability and rejection performance were prepared via mussel inspired PNIPAm grafting.



Thermo responsive ultrafiltration membranes of grafted poly(*N*-isopropyl acrylamide) via polydopamine

Bijay P. Tripathi,^{*a} Nidhi C. Dubey,^{a,b} F. Simon,^a and M. Stamm^{*a,b}

^a*Department of Nanostructured Materials, Leibniz Institute of Polymer Research Dresden, Hohe Str. 6, D-01069 Dresden, Germany.*

^b*Technische Universität Dresden, Department of Chemistry, Dresden 01069, Germany.*

Tel: +49-3514658324; Fax: +49-3514658281; E-mail: tripathi@ipfdd.de; bijayptripathi@yahoo.com; stamm@ipfdd.de

Commercial poly(ethylene terephthalate) (PET) microfiltration (MF) membranes have been modified with thermo responsive poly(*N*-isopropylacrylamide) (PNIPAm) via polydopamine. At first, dopamine was self-polymerized under wet conditions. Then, the amino-terminated PNIPAm was grafted by its amino group on the reactive polydopamine layer in aqueous solution. X-ray photoelectron spectroscopy (XPS) was used to study the chemical structure of the membrane surface, which confirmed the successful introduction of polydopamine and immobilization of PNIPAm molecules. Changes in surface morphologies after modification were investigated by means of scanning electronic microscopy (SEM). The wetting behavior of membranes was characterized by dynamic contact angle measurements. Finally the membranes were investigated for pure water flux, rejection, antifouling behavior, and water flux recovery to assess suitability for filtration and separation applications. Separation properties of these membranes depend on temperature because of thermoresponsive behavior of PNIPAm. Flux strongly increases with temperature, fouling is reduced and recovery from fouling is significantly improved.

Keywords: Track etched membrane, thermo responsive membrane, polydopamine, poly(*N*-isopropylacrylamide), and protein separation.

1. Introduction

In recent years, stimuli-responsive polymeric-based membranes have received a lot of interest from various scientific field due to their potential applications in the fields of controlled drug delivery, chiral separation, bioseparation, water treatment, chemical sensor or valve applications, tissue engineering and so on.¹⁻³ Stimuli responsive membranes can dramatically change flux or rejection in response to small chemical or physical stimuli in their environments such as temperature, pH, ionic strength, light, magnetic field and/or chemicals.⁴⁻¹¹ Among environmental stimuli-responsive membranes, a special interest has been given to thermo-responsive membranes since, in many cases, the temperature variation is important and it can easily be manipulated artificially. Several techniques have been used to prepare temperature sensitive polymeric based membranes such as the vacuum filtration method,¹² the adsorption method,¹³ the coating method,¹⁴ by the introduction of nanosized thermoresponsive particles into the membranes,¹⁵ polymerization of monomers within pores,^{1,16} or by simply grafting thermoresponsive polymers onto porous membranes substrates by different grafting techniques.¹⁷⁻²⁰

Poly(*N*-alkylacrylamide)s are some of the most studied responsive polymers with poly(*N*-isopropylacrylamide) (PNIPAm) being the most studied one of the group of temperature-responsive polymers. In aqueous solution, PNIPAm has a lower critical solution temperature (LCST) of 31-32 °C. At this temperature in water PNIPAm undergoes a phase transition, reversibly precipitating above this LCST and dissolving below this LCST. The volume-phase transition property of PNIPAm in membrane pores can be used to make the pore size tunable and the convective flow or solute diffusion through membrane pores can be controlled or switched. The temperature responsive tunability of PNIPAm based surfaces also lead to the switching of hydrophilic-hydrophobic properties. Surface grafted PNIPAm causes temperature-dependent changes in the physicochemical surface properties toward higher hydrophobicity above the

LCST.²¹ In protein adsorption studies of systems consisting of PNIPAm, in general more adsorption was observed above the LCST because of the higher hydrophobicity of the PNIPAm chains.²² This property is highly beneficial for membranes in protein separation technology.

A variety of strategies have been studied to generate thermoresponsive membranes by grafting PNIPAm or PNIPAm-based polymers onto membrane surfaces. The main strategies for grafting of PNIPAm on polymeric supports are based on free radical polymerization,²³ plasma-induced polymerization,²⁴ photografting,^{19,25} corona discharge,²⁶ and so on. In recent years, several reports deal with atom transfer radical polymerization or photo-induced reversible addition-fragmentation chain transfer graft copolymerizations.^{18,27,28} Recently, the attachment strategy based on catecholic chemistry has gained renewed interest because of the work on polymerized catecholic amine (polydopamine).²⁹ This strategy has received considerable attention to develop antifouling membranes by surface modification.³⁰⁻³² Polydopamine also used for grafting of polymers, biomolecules, ATRP processes, etc.³³⁻³⁸ These results motivated our interest to modify the polydopamine modified surface by grafting of thermo responsive units and study the separation and fouling properties. Membranes modified with polydopamine enhance the water flux due to the increased hydrophilicity caused by the hydroxyl groups on their surfaces.³⁰ Post modifications of polydopamine surfaces are possible via Schiff base or Michael addition reactions which offer the opportunity to attach amine or thiol containing compounds.³⁹ The self-assembly of dopamine and subsequent grafting of functionalized polymers in aqueous media makes the process environmentally friendly.

Herein we report a simple approach for the fabrication of thermoresponsive membranes by surface and pore medication via mussel inspired surface chemistry. Dopamine was first self-polymerized on the surface and pore walls of PET track etched membranes and amino terminated PNIPAm were grafted on polydopamine layer to introduce the thermoresponsive properties. The

prepared membranes were thoroughly characterized for their chemical structure, microscopic and surface properties, thermoresponsive character, water permeation, protein rejection, and antifouling ability.

2. Experimental section

2.1. Materials

Commercial PET track-etched membranes (diameter: 47 mm, pore size: 0.3-0.4 μm , pore density: 1.5×10^8 pores/cm²) were obtained from it4ip (Seneffe, Belgium). Amino-terminated poly(N-isopropylacrylamide) (molecular weight: 6400; PDI: 1.51) was purchased from Polymer Source Inc. (Quebec, Canada). All other chemicals were obtained from Sigma-Aldrich, Inc. (St. Louis, Missouri, USA) and used as received. For all purpose Millipore water was used.

2.2 Preparation of membranes

PET track-etched membranes were soaked in water-ethanol and washed several time to remove impurities and contaminations. To obtain a dopamine solution of 2.0 mg mL⁻¹, dopamine [4-(2-aminoethyl)benzene-1,2-diol] was dissolved in a mixed solvent made from 10 mmol L⁻¹ tris-HCl buffer solution (pH 8.5, tris = 2-amino-2-hydroxymethyl-propane-1,3-diol) and ethanol ($V_{\text{tris}}:V_{\text{ethanol}} = 9:1$). Cleaned and wet PET membranes were immersed in dopamine solution. The reaction vessel containing the reaction mixture was placed on a shaker and kept there at room temperature for 4 h. The polydopamine-coated membranes were carefully washed with ethanol and deionized water. Finally they were dried at 60 °C in vacuum.

Polydopamine-coated membranes were immersed into a solution of amino-terminated PNIPAm (2.0 mg mL⁻¹) dissolved in 15 mmol L⁻¹ tris-HCl buffer (pH 8.5). The grafting reaction took place under slight shaking at 60 °C for 3 h. After cooling down to room temperature, the membranes were further kept on shaker for 12 and 24 h. The modified membranes were thoroughly washed with deionized water and dried in vacuum at 60 °C to constant mass. The

polydopamine and PNIPAm modified membranes were denoted as PET-D and PET-NX, respectively, where X is the time (12 and 24h) allowed for PNIPAm grafting.

The amounts of dopamine and PNIPAm grafted to the PET membrane substrates were determined by weighing the membranes before and after the surface modification process. The degree of immobilization (γ) was calculated according to equation (1)

$$\gamma = \frac{W - W_0}{W_0} \cdot 100 \% \quad (1)$$

where W and W_0 represents the weight of the membrane after and before modification with dopamine and PNIPAm.

2.3. Characterization methods

2.3.1. X-Ray photoelectron spectroscopy (XPS)

XPS is a very surface-sensitive analytical method. Hence, XPS seemed to be a suitable analytical technique to study chemical changes on the differently treated membrane surfaces. XPS analysis was performed using an Axis Ultra spectrometer (Kratos Analytical, Manchester, U.K.) equipped with a monochromatic Al $K\alpha$ X-ray source of 300 W at 20 mA. The kinetic energy of the photoelectrons was determined with a hemispheric analyzer set to pass energy of 160 eV for the survey spectra and of 20 eV for high-resolution spectra. During all measurements electrostatic charging of the sample was avoided by means of a low-energy electron source working in combination with a magnetic immersion lens. Later, all recorded peaks were shifted by the same amount which was necessary to set the C 1s peak to 284.70 eV for unsaturated hydrocarbon atoms of the phenyl rings. During all measurements the base pressure in the analysis chamber was less than 10^{-8} mbar. Quantitative elemental compositions were determined from peak areas using experimentally determined sensitivity factors and the spectrometer transmission function. Spectrum background was subtracted according to Shirley.⁴⁰ The high-resolution spectra were

deconvoluted by means of a computer routine (Kratos Analytical, Manchester, UK). Free parameters of component peaks were their binding energy (BE), height, full width at half maximum and the Gaussian-Lorentzian ratio.

2.3.2. Dynamic contact angle measurements

The wetting behavior of the membranes was studied employing the optical contact angle measurement system OCA40 (Data Physics, Bad Vilbel, Germany). Contact angles were measured by sessile drop experiments as advancing (θ_{adv}) and receding (θ_{rec}) contact angles. Deionized water droplets having a surface tension of 72.8 mN m^{-1} were placed on the sample surface by a motor-driven syringe.⁴¹ After gradual increases of the droplet volume (the droplet volume was varied between 2 and 8 μL advancing contact angle values (θ_{adv}) were measured. The variation in the measured values was within $\pm 2^\circ$, and the values reported are averages of at least three measurements. These contact angle values reflect the wetting behavior of the sample surface. Receding contact angle values (θ_{rec}) measured after gradual decreases of the droplet volume characterize the dewetting behavior. The difference between advancing and receding contact angle values gives the contact angle hysteresis ($\Delta\theta = \theta_{adv} - \theta_{rec}$).^{42,43} The free energy values of the solid-liquid interface ($-\Delta G_{sl}$) were calculated from the advancing contact angle values using a water surface tension value of 72.8 mJ m^{-2} .^{41,43}

2.3.4. Scanning electron microscopy (SEM)

Surface and cross-section morphologies were obtained by scanning electron microscopy (SEM) using a NEON 40 FIB-SEM workstation (Carl Zeiss AG, Oberkochen, Germany) operated at 3 kV, after 3 nm thick sputter coating of platinum. Cross-section images were obtained after breaking the membranes in liquid nitrogen.

2.4. Membrane filtration experiment and pore size determination

Permeability and rejection test were conducted in a stirred cell filtration device (Catalogue number XFUF04701, Millipore, effective membrane area 15.18 cm²) connected with a nitrogen gas cylinder and solution reservoir. Pure water flux was determined for each membrane at pressures ranging from 0.1 to 1 bar. Before actual flux measurements, the membranes were pressurized at 3 bar for 15 min to open any blocked pores. The water flux is defined as:

$$J_w = \frac{V}{A \cdot \Delta t} \quad (2)$$

where V (L) was the volume of permeated water, A (m²) was the membrane area and Δt (h) was the permeation time. Temperature-dependent flux was measured from 20 to 60 °C. The temperature was controlled by a water bath.

Water flux data were also used to estimate the effective pore radius of the prepared membranes using the Hagen–Poiseuille equation:⁴³⁻⁴⁵

$$J_w = \frac{\varepsilon \cdot r^2}{8 \cdot \eta \cdot D \cdot \tau} \cdot \Delta p \quad (3)$$

where J_w is the volume flux, ε is the porosity, r is the average pore radius, η is the dynamic viscosity of water, D is the thickness of the membrane, τ is the membrane tortuosity, and Δp is the pressure drop through the membrane. For uniform cylindrical pores, ε can be calculated with the help of following equation:^{46,47}

$$\varepsilon = \frac{n_p \cdot \pi \cdot r^2}{A_m} \quad (4)$$

where n_p is the number of pores and A_m is the external membrane area.

Bovine serum albumin (BSA) protein was used to evaluate the membrane separation performance with the filtration setup, which was used for water flux measurements. The experiment was carried out at room temperature and 45 °C. The BSA concentration in feed (C_f) and permeate (C_p) was obtained by UV-vis spectroscopy. Concentration polarization on the

membrane surface was minimized by vigorous stirring to the solution over membrane. The experiment was repeated three times and permeates, 5.0 mL each, was collected. The BSA rejection (R) was calculated using following equation:

$$R = \left(1 - \frac{C_p}{C_f} \right) \times 100 \% \quad (5)$$

2.5. Fouling and flux recovery studies

The fouling behavior of the modified membrane was assessed by quantitative protein adsorption experiment. Piece of membrane with known area was dipped into the BSA aqueous solution (1 mg·mL⁻¹; pH 7). under constant shaking for 4 h. The difference in BSA concentration was estimated by UV-vis spectroscopy. The apparent amount of BSA adsorbed on the membranes surface (BSA adsorption capacity γ_{BSA} [$\mu\text{g cm}^{-2}$]) was calculated using the following equation:

$$\gamma_{BSA} = \frac{C_0 - C_f}{A} \quad (6)$$

where C_0 and C_f are the BSA concentration in the original and final solution, A is the area of the membrane used for the adsorption process.

Ultrafiltration (UF) experiments were conducted at room temperature with a stirring speed of 300 rpm to evaluate the antifouling behavior of developed membranes by passing 100 ml of 1 mg ml⁻¹ BSA solution at pH 7 and 1 bar pressure. After the UF of BSA solution, the membranes in UF cell were cleaned thoroughly by deionized water for 30 min. Then, under similar conditions pure water flux was measured again on the fouled membrane. The flux recovery percentage (FR [%]) of the membranes was calculated according to the following equation:⁴⁸

$$FR = \frac{J_v}{J_w} \cdot 100 \% \quad (7)$$

where J_w is the pure water flux of sample membrane before fouling and J_v is the pure water flux after fouling. The higher value of FR is an indicator for the better antifouling property of the

membranes. To examine the antifouling properties of prepared membranes in detail, several sets of equations were employed to describe the different parameters (Eqs. 8-10). The total fouling ratio (R_t), reversible fouling ratio (R_r), and irreversible fouling ratio (R_{ir}) were determined using following equations:⁴⁸⁻⁵⁰

$$R_t = \frac{J_w - J_p}{J_w} \cdot 100 \% \quad (8)$$

$$R_r = \frac{J_v - J_p}{J_w} \cdot 100 \% \quad (9)$$

$$R_{ir} = \frac{J_w - J_v}{J_w} \cdot 100 \% \quad (10)$$

where J_p is the protein flux.

3. Results and Discussion

3.1. Membrane preparation

In this work, PET track etched membranes were used as micro porous support to anchor thermo responsive PNIPAm on the surface and inside the pores via mussel inspired surface chemistry. The detail membrane preparation steps and grafting reaction are depicted in Fig. 1. Firstly, dopamine was polymerized by pH-induced oxidation at room temperature. It is reported that dopamine is more effective in improving the surface hydrophilicity and water permeability when it is utilized for surface modification of polymeric membranes.³⁷ Also, polydopamine allows further covalent immobilization of molecules and polymers containing free amine groups. Thus the polydopamine was used as surface modifier of PET track etched membrane and as intermediate active layer to graft PNIPAm for achieving thermo responsive membranes. We believe that the attachment of polydopamine to the membrane was by physical interactions. An indication of the polydopamine deposition on a substrate is given by the darkening color with

growth time due to the strong UV-visible absorption.⁵¹ Polydopamine coated membranes were thoroughly washed with water and ethanol to remove any non-reacted dopamine and dried in vacuum at 60 °C overnight. The color of polydopamine coated membranes changes from deep brown to gray with grafting of PNIPAm. Thus obtained dried polydopamine modified membranes were kept in amino terminated PNIPAm aqueous solution (2 mg mL⁻¹ in tris-buffer) for spontaneous grafting. Fig. 2 indicates the changes in physical appearance of PET membrane with deposition of polydopamine and grafting of PNIPAm. The mass gain of each sample after the dopamine polymerization and subsequent PNIPAm grafting was analyzed gravimetrically and the degree of immobilization/grafting (DG) was calculated. The data are presented in Table 1, and revealed that the PNIPAm grafting was time dependent. However, the relative PNIPAm grafting was higher in the first 12 h (for PET-N12 membrane) as compared to the next 12 h (for PET-N24 membrane).

3.2. Chemical structure of the modified membrane surfaces

In order to study the chemical structure of the modified PET membranes X-ray photoelectron spectroscopy (XPS) was employed. The recording of high-resolution element spectra allowed analyzing the different binding states of the elements forming the surface layer, which was in contact to the fluid medium during the membrane separation process.⁵² The left column in Fig. 3 shows a series of wide-scan spectra recorded from the differently treated PET track-etched membranes. As can be seen in Fig. 3a, beside the expected elements carbon (C 1s peak) and oxygen (O1s, O 2s and O Auger series) the unmodified PET support surface also contains a considerable amount of nitrogen (N 1s peak; [N]:[C] = 0.028). The nitrogen originates from a commercially applied thin coating layer made from poly(*N*-vinylpyrrolidone) (PVP), which increases the hydrophilicity of the PET material and the wettability of the membrane towards polar liquids. The shape of the corresponding C 1s spectrum is very typical for PET (Fig. 3a,

middle column). Clearly, it shows the three component peaks resulting from the PET structure. Component peak *Ph* at 284.70 eV shows the carbon atoms of the phenyl rings ($-\text{HC}=\text{CH}- \leftrightarrow =\text{HC}-\text{CH}=\text{}$) of the PET polymer. Saturated hydrocarbons (C_xH_y) of the PVP polymer and non-specifically adsorbed surface contaminations, which are usually present on surfaces, also contribute to component peak *Ph*. The observation of *shake-up* peaks (at 291 eV and 295 eV), which result from π -electron transitions between π and π^* orbitals, confirm the presence of the conjugated π -electron system of the phenyl rings. Component peak *E* at 288.68 eV arose from carbonyl atoms of PET's carbonic ester groups ($\text{O}=\text{C}-\text{O}-\text{C}$). The corresponding alcohol-sided carbon atoms of the carbonic ester groups were observed as a part of component peak *C*. The presence of PVP molecules on the sample surface was detected by the two additional component peaks *B* and *D*, which were necessary to fit the calculated cumulative curve (sum of all component peaks) to the recorded C 1s spectrum. Component peak *D* (287.21 eV) shows carbonyl carbon atoms of the PVP's inner amide groups ($\text{O}=\text{C}-\text{N}[-\text{C}]_2$). Its intensity equalled the $[\text{N}]:[\text{C}]_{\text{spec}}$ ratio, which was independently determined from the wide-scan spectrum. The corresponding amine-sided carbon atoms ($\text{O}=\text{C}-\text{N}[-\text{C}]_2$) contributed (with the double intensity of component peak *D*) to component peak *C*. Component peak *B* shows carbon atoms in α -position to the carbonyl carbons of the amide groups ($\text{H}_2\text{C}-\text{C}[\text{O}]\text{N}[-\text{C}]_2$). The intensity of component peak *B* equalled the intensity of component peak *D*. The high-resolution N 1s of the unmodified PET track-etched membrane shows only one component peak *K* at 399.52 eV. The binding energy of component peak *K* is typical for nitrogen atoms involved in amide groups ($\text{O}=\text{C}-\text{N}[-\text{C}]_2$). Since the amide groups of PVP cannot be protonated an additional component peak showing protonated nitrogen species, which is usually observed for amino groups, was not detected.

After polymerizing dopamine on the PET track-etched membrane surface the relative nitrogen content ($[N]:[C]$) is significantly increased, while the relative oxygen content remains constant (Table 2). The C 1s spectrum of the PET-D sample is characterized by an intensive shoulder at ca. 286 eV and an increased intensity of the *shake-up* peaks at ca. 291 eV (Fig. 3b, middle column). The intensive shoulder at 286 eV results from the applied polydopamine layer where the phenolic C–OH groups of the catechol rests contributed to component peak C (286.23 eV), and the cyclic amine bonds ($\underline{C}-\underline{NH}-\underline{C}$ and $\underline{C}-\underline{N}=\underline{C}$) increased the intensity of component peak B (285.63 eV). However, the intensity of component peak B was significantly smaller as the double of the $[N]:[C]_{\text{spec}}$ ratio, which was determined from the wide-scan spectrum of the PET-D sample. Obviously, a considerable amount of nitrogen is involved in amide groups, which were observed as component peak D (BE = 287.52 eV). The origin of the two component peaks Ph and E was explained above. The wide and intensive *shake-up* peaks observed in the C 1s spectrum of the PET-D sample corresponds to the chemical structure of the polydopamine layer, which is characterized by a highly conjugated π -electron system. With increasing the number of conjugated p-electrons the number of possible linear combinations (π and π^* orbitals) is increased, and each linear combination reduces the energy gap between π and π^* orbitals. Hence, $\pi \rightarrow \pi^*$ electron transitions between π and π^* orbitals will be more probable. Surprisingly, the high-resolution N 1s spectrum of the PET-D sample clearly shows three component peaks X, K, and L (Fig. 3b, right column). Component peak K (399.64 eV) results from C– \underline{N} bonds of the cyclic amino groups (C– \underline{NH} –C) of the attached polydopamine. As mentioned above C– \underline{N} bonds of amide groups (O=C– \underline{NH} –C) also contributed to component peak K. Component peak L (401.46 eV) arose from nitrogen atoms of protonated amino groups (C– $\underline{N}^+\text{H}_2$ –C). It can be considered as proof that amino groups are present on the sample surface because amide groups did not show the protonation/deprotonation equilibrium as can be seen in the N 1s spectrum

recorded from the PET track-etched membrane (Fig. 3a, right column). The binding energy found for component peak *X* (398.17 eV) seems to be small for organically bonded nitrogen. Obviously, the double bond in the cyclic imine group (C–N=C) increases the electron density on the nitrogen atom and shifts the binding energy to lower values.

After grafting the PNIPAm polymer on the polydopamine layer, the shape of the high-resolution N 1s spectrum was not significantly changed (Fig. 3c, right column). Component peak *K* shows the presence of cyclic amino groups and carbonic amides. Photoelectrons that escaped from the nitrogen of protonated amino groups contributed to component peak *L*. The intensity of component peak *X* is slightly decreased because the attached PNIPAm molecules cover the sample surface. The grafting of PNIPAm introduced additional amide groups and increased the relative nitrogen content [N]:[C] on the sample surface slightly (Table 2). In the high-resolution C 1s spectrum the amine-sided carbon atoms of the PNIPAm's amide groups (O=C–NH–C[CH₃]₂) increased the intensity of component peak *B* (285.68 eV, Fig. 3c, middle column). The corresponding carbonyl atoms (O=C–NH–C[CH₃]₂) contributed with the same intensity to component peak *D* (287.52 eV). Due to the covering the polydopamine surface by the PNIPAm molecules the intensity of the *shake-up* peaks at 291 eV is slightly decreased. The origin of the other component peaks is explained above.

3.3. Membrane morphology and contact angle measurements

Fig. 4 depicts the surface and cross-section SEM images of the PET membrane and the membranes modified with polydopamine and PNIPAm. As expected the diameters of pores of the modified membranes were reduced with modification. It can also be observed that the PET track-etched membrane surface was relatively smooth and no cracks or deformations were observed. However, for the polydopamine-coated membrane, the surface became rough and numerous nano-scaled particles were observed. This roughness of polydopamine-coated membrane could be

due to the polymerization process of dopamine.³² After the grafting of PNIPAm on polydopamine-coated membrane, the surface again became smooth which indicates the homogenous grafting and coverage of surface. The pore size of the membrane was reduced after PNIPAm grafting and some of the pores were getting covered in PET-N24 membrane due to high degree of grafting. Cross-section images of dopamine polymerized (Fig. 4E) and PNIPAm grafted (Fig. 4 F) membranes indicate that the pores were intact and no blockage was observed. The surface and cross-section images also indicate that the grafting of PNIPAm was much more prominent than inside the pores. The blockage of some of the pores openings only on surface proves this point. The high degree of PNIPAm grafting on the membrane surfaces as compared to the pore walls give an anisotropic pore structure.

The wetting behavior of the differently prepared membranes was characterized by dynamic contact angle measurements using deionized water as test liquid. Table 1 summarizes the advancing (θ_{adv}) and receding contact angles (θ_{rec}). In contrast to pure PET the PVP-coated non-treated PET track-etched membrane has a hydrophilic surface. The hydrophilicity was improved by the modification with polydopamine. The high number of polar surface groups, such as phenolic OH-groups and cyclic amino groups lowered the advancing as well as receding contact angle values. The additional grafting of the PNIPAm polymer did not significantly affect the advancing contact angle but the receding contact angle value was significantly decreased. While the advancing contact angle values characterize the wetting behavior of a dry surface, the receding contact angle is the characteristic value to quantify the dewetting of surface, which was in contact with a liquid. Differences in the advancing and receding contact angles, commonly called contact angle hysteresis ($\Delta\theta$), reflect the work of adhesion (modulus of the interaction free energy ΔG_{sl}) resulting from interactions between the solid surface and the applied water molecules. Dynamic effects taking place on the wetted surfaces, such as swelling and the

reorganization of polymer chains increase the work of adhesion. In addition, surface roughness resulting from the porous surface structure also contributes to the contact angle hysteresis.⁵³ The increase of the contact angle hysteresis after grafting the PNIPAm indicates a high molecular mobility of the PNIPAm sequences in presence of water. These findings seem to be important to control the net water content of the membrane, which has high impact on its swelling, stability, and fouling properties.

3.4. Water flux, temperature response, and pore size determination

The water flux for membranes with polydopamine modification and varied degree of PNIPAm grafting was measured in a typical laboratory dead-end filtration device. The effect of pressure on water permeation through the membrane is depicted in Fig 5. A linear increase of the flux in pure water was observed with increasing trans-membrane pressure. However, the modified membranes showed lower flux values compared to the normal PET membranes, which can be explained due to the additional thickness imparted by the modification of film. The SEM pictures also indicate intact pores of PET membranes with some surface coverage. It was also observed that the decrease in water flux value in lower pressure range was less prominent compared to higher pressure.

The effect of temperature on the flux of water through the temperature-sensitive membrane is shown in Fig. 6. For comparison, the water flux of the nascent membrane is also given in Fig. 6. It is clear that the water flux through the temperature-sensitive membrane depends little on the temperature when the temperature is lower than 30 °C. However, when the temperature was higher than 32 °C, due to the LCST of PNIPAm, water flux increases significantly with the rise of temperature. The pure water flux was increased almost two fold increasing the temperature from 20 °C to 45 °C. Meanwhile, as expected, the water flux through the nascent PET membrane was not affected by temperature change because the structure of the

membrane will remain unchanged in the range of temperature from 20 °C to 45 °C. A slight increase in water flux for PET-D membrane was observed with increasing temperature, which may be due to increased hydrophilicity of polydopamine layer on the membrane.³⁸

The net water flux for polydopamine coated membrane was slightly higher at 45 °C compared to the base membrane. The change in grafted PNIPAm layer is also schematically represented in Fig. 6. A pore opening and closing phenomenon can be postulated to be responsible for the change in water flux with the change in temperature. The PNIPAm layer absorbs large amount of water molecules below LCST which lead to extension of the polymer chain. This shrinks the effective pore size of the PNIPAm grafted membrane. Whereas the deswelling occurs above LCST which leads to the shrinkage in polymer chain length and the increase in effective pore radius. Thus, the pores of PNIPAm grafted membranes can be regarded as temperature switchable valves which can regulate the transport of water as well as small molecules according to the temperature.

The hydrodynamic pore diameters at 20 °C (swollen state) and 45 °C (collapsed state) were calculated with Hagen-Poiseuille's law assuming that water flow through the swollen grafted PNIPAm polymer layer can be ignored.³ The calculation was based on pure water flux and porosity data. The number of pores per unit of area was obtained by direct counting method in SEM images of respective membranes. The number of pores per cm² was in close agreement with supplier data and 1.75×10^8 pore/cm² was counted by averaging the numbers from 10 different places in SEM image. The data presented in Fig. 7 clearly indicate that the apparent hydrodynamic pore size for both temperatures decreased with polydopamine coating and PNIPAm grafting. The small change in pore size for PET and PET-D membranes can be explained due to the increased water permeation at high temperature. The obtained pore size for PET membrane was smaller than the supplier data. This difference can be explained due to

different reasons such as pore counting and water flux data. The change in pore size for PNIPAm grafted membranes was quite prominent with temperature. The pore size reduction with increasing grafting time at 20 °C was observed but there was almost no difference at 45 °C. Reduction in pore size of the PET track etched membrane to an appropriate value leads to the fabrication of ultrafiltration membranes.

To examine the stability of the grafted PNIPAm layers in the membrane pores in long-term operations, the repeatability of thermo-responsive “open-close” gating of grafted membranes (PET-N24) was investigated and the results are shown in Fig. 8. The water flux was measured at 20 and 45 °C alternatively for repeated five cycles. The flux values at both temperatures for repeated cycles were almost constant. However, a small increase in water flux was noticed with the progress of experiment, which may be due to the loss of some loosely bonded PNIPAm molecules or opening of closed pores. Overall, the membrane showed good thermo responsive repeatability and can be well regarded as a membrane with thermo switching gates.

3.5. Ultrafiltration of protein and antifouling performance

The significant change of effective pore size on the surface of the temperature-sensitive membrane makes it possible to separate chemical species and biomolecules with different sizes. To evaluate the effect of modification on protein separation behavior, BSA protein was filtered through the membranes at RT and 45 °C, and the rejection data are plotted in Fig. 9. The microscopic characterization, water flux, and pore size determination of membranes showed that the pore size of the membranes was decreased with each modification step and also exhibited thermal switchability. Thus the protein rejection tendency was increased for modified membranes compared to PET. Although BSA molecular sizes (hydrodynamic radius about 8 nm) are far smaller than the membrane pore size, many molecules are retained in the used membranes. The

BSA rejection for unmodified membrane was quite low but it was more than 80% for PNIPAm modified membranes in all conditions. The high rejection can be attributed to the BSA aggregate formation in the suspension. Many BSA aggregates are retained by the membrane by the so-called “sieving effect”. The BSA rejection is therefore more as more aggregates are deposited onto the membrane surfaces. The rejection for polydopamine modified membrane was slightly higher than neat PET membrane which may be due to pore size reduction and attachment of BSA molecules on the polydopamine layer. BSA molecules contain a large number of amine functionality which could covalently attach on the membrane surface and in the pores, resulting in the lowering the protein concentration in solution as well as a reduction of the pore size of the membrane.⁵⁴ PNIPAm modification ruled out the possibility of BSA attachment on membrane surface via polydopamine layer. The protein rejection for PNIPAm modified membranes was higher than neat and polydopamine modified PET membranes. It is well known that below LCST, PNIPAm chains are in extended chain conformation condition with large number of water molecules attached and repel protein.⁵⁵ The extension of PNIPAm chains reduces the size of the membrane pores and also the presence of water in PNIPAm chains hinders the protein adsorption and penetration. The property of hydrophilic PNIPAm layer to resist protein adsorption can be attributed to high steric repulsion and water structuring/hydration forces. Thus very low transmission of BSA was feasible with PNIPAm grafted membranes and more than 80% rejection was observed for the PET-N24 membrane at RT. The rejection value at 45 °C was lower than at RT for all membranes. This was due to the thermo switching behavior of pores of the PNIPAm grafted membranes as well as due to the conformational changes of the BSA protein. At higher temperature, PNIPAm adopts a more hydrophobic state because of structural changes above its LCST.^{21,56} This allows the protein molecules to penetrate the surface PNIPAm layer and get

transmitted through the pores. Thus a low rejection was reported for BSA at 45 °C operation temperature.

In current separation and filtration membranes, the most important problem is organic and biofouling. Adsorption of organic matter leads to the formation of layers on membrane surface and blockage of pores, which further facilitates microorganism growth and biofilm formation. Thus, for long term use of membranes, high antifouling properties are required. In this study, fouling on membrane surface was studied by simple protein adsorption experiment. Membrane coupons of definite area were kept in BSA protein solution under constant shaking for BSA adsorption and the remaining concentration in bulk solution was obtained by UV-vis measurements at 280 nm. The polydopamine modified membrane showed highest protein adsorption in given environmental condition. The high adsorption can be explained due to electrostatic interaction and the possibility of a reaction between dopamine and the protein. The BSA adsorption on PNIPAm modified membranes was quite low as compared to PET and PET-D membranes. PNIPAm surfaces are known for their protein resistive nature due to the presence of large amounts of water molecules in the vicinity of hydrophilic part below LCST.^{21,56} Above LCST, the PNIPAm chains collapse due to dissociation of water and the surface become hydrophobic. PNIPAm surface adsorbed significantly more proteins above its LCST than below it. Similar results were observed in this case also, where high protein adsorption above LCST and low adsorption below LCST can be seen in Fig. 10. As discussed above, the unfolding of BSA molecules occurs at high temperature, where the functional groups are exposed and aggregating and accumulating on the surface starts. In addition, the unfolding of the BSA molecule at higher temperature exposes the hydrophobic residues and increases the hydrophobic interactions between BSA molecules that lead to higher rate of aggregation.⁵⁷ The data in Fig. 10 revealed that the BSA adsorption at 45 °C was similar for both PNIPAm containing membranes. Thus, the

PNIPAm grafting on membrane surfaces is beneficial not only in thermal switching but also provides high antifouling ability below LCST.

The low BSA adsorption and thus low fouling tendency on modified membrane surfaces was further confirmed by recording the water flux recovery after filtration of BSA solution at 20 and 45 °C. After BSA filtration, membranes were thoroughly cleaned with deionized water and pure water fluxes (J_V) were measured again. From J_W and J_V , the flux recovery (FR) rates were calculated and depicted in Fig. 11. The FR rates are an indicator for the reversing of fouling and indicate that the adsorbed protein can be removed to a large extent by proper washing. PNIPAm grafted membranes showed more than 80% flux recovery at both investigated temperatures. The lowest FR was observed for polydopamine modified membranes, which indicates that the adsorbed BSA was quite firmly bonded with the surface and removal by simple cleaning methods was not possible. The temperature effect was also clearly visible and low recovery was observed at 45 °C compared to 20 °C.

The fouling behavior of developed membranes was further evaluated in detail by determining R_t , R_r , and R_{ir} values (Fig. 12). It is evident from the figure that the R_t was systematically reduced with PNIPAm grafting. The reversible protein fouling with PNIPAm grafting was reduced which led to the decrease in percentage of the irreversible fouling ratio. The lowest irreversible fouling was achieved for PET-N24 membranes due to protein resistive nature of hydrophilic PNIPAm layer below LCST. Overall, the low total fouling and irreversible fouling ratio for the membrane PET-N24 can be explained by assuming that the protein fouling layer could be removed easily by simple cleaning with water what is highly beneficial for a more effective UF process.

4. Conclusions

We could show that our approach to functionalize membranes under mild conditions with the temperature-responsive polymer, PNIPAm, leads to a temperature responsive membrane. A porous base membrane from technical polymers can be functionalized in an easy and controlled way by using polydopamine as mediating layer. Track-etched PET membranes were first functionalized with polydopamine followed by grafting of amino terminated PNIPAm under mild basic conditions. The self-polymerization of polydopamine on the membrane surface and further grafting of PNIPAm on the polydopamine layer was confirmed by XPS, microscopic characterization, and contact angle measurements. A reduction in pore size was observed with each modification step but the pores remained intact. The thermo responsive character was proved by determining the water permeability and protein rejection under varying solution temperature. Protein adsorption and fouling tendency depends upon temperature due to conformational changes of the PNIPAm layer. The membrane separation performance was evaluated for the model protein BSA and more than 80% rejection was recorded. The water flux recovery, reversible and irreversible fouling, and protein adsorption data indicate that the prepared membranes exhibited good antifouling ability.

The results confirm that polydopamine can be used as a precursor layer to graft various functionalized molecules and polymers to obtain smart and switchable membranes. The self-polymerization tendency of dopamine under mild condition on various substrates makes an interesting choice for surface modification and further grafting applications.

Acknowledgements

B.P. Tripathi acknowledges Alexander von Humboldt Foundation for AvH Postdoctoral Fellowship.

References:

- [1] M. Temtem, D. Pompeu, T. Barroso, J. Fernandes, P. C. Simões, T. Casimiro, A. M. Botelho do Rego and A. Aguiar-Ricardo, *Green Chem.*, 2009, 11, 638.
- [2] R. Xie, L. Chu, W. Chen, W. Xiao, H. Wang and J. Qu, *J. Membr. Sci.*, 2005, 258, 157-166.
- [3] S. Frost and M. Ulbricht, *J. Membr. Sci.*, 448 (2013) 1-11.
- [4] I. Tokarev and S. Minko, *Adv. Mater.*, 2010, 22, 3446-3462.
- [5] P.-F. Li, R. Xie, J.-C. Jiang, T. Meng, M. Yang, X.-J. Ju, L. Yang and L.-Y. Chu, *J. Membr. Sci.*, 2009, 337, 310-317.
- [6] A. L. Allen, K. J. Tan, H. Fu, J. D. Batteas and D. E. Bergbreiter, *Langmuir*, 2012, 28, 5237-5242.
- [7] S. P. Nunes, R. Sougrat, B. Hooghan, D. H. Anjum, A. R. Behzad, L. Zhao, N. Pradeep, I. Pinnau, U. Vainio and K.-V. Peinemann, *Macromolecules*, 2010, 43, 8079-8085.
- [8] Y. S. Park, Y. Ito and Y. Imanishi, *Langmuir*, 1998, 14, 910-914.
- [9] G. Brisson, M. Britten and Y. Pouliot, *J. Membr. Sci.*, 2007, 297, 206-216.
- [10] Y. Ito, M. Inaba, D. J. Chung and Y. Imanishi, *Macromolecules*, 1992, 25, 7313-7316.
- [11] Y. S. Park, Y. Ito and Y. Imanishi, *Macromolecules*, 1998, 31, 2606-2610.
- [12] S.-Y. Lin, C.-J. Ho and M.-J. Li, *J. Controlled Release*, 2001, 73, 293-301.
- [13] S.-Y. Lin, H.-L. Lin and M.-J. Li, *J. Membr. Sci.*, 2003, 225, 135-143.
- [14] J.-P. Chen, Y.-M. Sun and D.-H. Chu, *Biotechnol. Progr.*, 1998, 14, 473-478.
- [15] K. Zhang and X. Y. Wu, *Biomaterials*, 2004, 25, 5281-5291.
- [16] N. Adrus and M. Ulbricht, *J. Mater. Chem.*, 2012, 22, 3088.
- [17] L.-Y. Chu, Y. Li, J.-H. Zhu and W.-M. Chen, *Angew. Chem. Int. Ed.*, 2005, 44, 2124-2127.
- [18] A. Friebe and M. Ulbricht, *Langmuir*, 2007, 23, 10316-10322.
- [19] C. Geismann and M. Ulbricht, *Macromol. Chem. Phys.*, 2005, 206, 268-281.

- [20] M. Mathieu, A. Friebe, S. Franzka, M. Ulbricht, N. Hartmann, *Langmuir*, 2009, 25, 12393-12398.
- [21] S. Burkert, E. Bittrich, M. Kuntzsch, M. Muller, K. J. Eichhorn, C. Bellmann, P. Uhlmann and M. Stamm, *Langmuir*, 2010, 26, 1786-1795.
- [22] H. Lakhari, T. Okano, N. Nurdin, C. Luthi, P. Descouts, D. Muller and J. Jozefonvicz, *Biochim. Biophys. Acta*, 1998, 1379, 303-313.
- [23] W. Minghong, B. Bao, J. Chen, Y. Xu, S. Zhou and Z.-T. Ma, *Radiat. Phys. Chem.*, 1999, 56, 341-346.
- [24] L. Liang, M. Shi, V. V. Viswanathan, L. M. Peurrung and J. S. Young, *J. Membr. Sci.*, 2000, 177, 97-108.
- [25] C. Geismann, A. Yaroshchuk and M. Ulbricht, *Langmuir*, 2007, 23, 76-83.
- [26] M. Hesampour, T. Huuhilo, K. Mäkinen, M. Mänttari and M. Nyström, *J. Membr. Sci.*, 2008, 310, 85-92.
- [27] Z. B. Zhang, X. L. Zhu, F. J. Xu, K. G. Neoh and E. T. Kang, *J. Membr. Sci.*, 2009, 342, 300-306.
- [28] I. Lokuge, X. Wang and P. W. Bohn, *Langmuir*, 2006, 23, 305-311.
- [29] H. Lee, S. M. Dellatore, W. M. Miller and P. B. Messersmith, *Science*, 2007, 318, 426-430.
- [30] S. Kasemset, A. Lee, D. J. Miller, B. D. Freeman and M. M. Sharma, *J. Membr. Sci.*, 2013, 425-426, 208-216.
- [31] L. Chen, R. Zeng, L. Xiang, Z. Luo and Y. Wang, *Analytical Methods*, 2012, 4, 2852.
- [32] C. Cheng, S. Li, W. Zhao, Q. Wei, S. Nie, S. Sun and C. Zhao, *J. Membr. Sci.*, 2012, 417-418, 228-236.
- [33] Y. B. Lee, Y. M. Shin, J. H. Lee, I. Jun, J. K. Kang, J. C. Park and H. Shin, *Biomaterials*, 2012, 33, 8343-8352.

- [34] J.-H. Jiang, L.-P. Zhu, X.-L. Li, Y.-Y. Xu and B.-K. Zhu, *J. Membr. Sci.*, 2010, 364, 194-202.
- [35] C. Y. Li, W. C. Wang, F. J. Xu, L. Q. Zhang and W. T. Yang, *J. Membr. Sci.*, 2011, 367, 7-13.
- [36] R. Luo, L. Tang, J. Wang, Y. Zhao, Q. Tu, Y. Weng, R. Shen and N. Huang, *Colloids Surf. B Biointerfaces*, 2013, 106, 66-73.
- [37] Z.-Y. Xi, Y.-Y. Xu, L.-P. Zhu, Y. Wang and B.-K. Zhu, *J. Membr. Sci.*, 2009, 327, 244-253.
- [38] J. I. Clodt, V. Filiz, S. Rangou, K. Buhr, C. Abetz, D. Höche, J. Hahn, A. Jung and V. Abetz, *Adv. Funct. Mater.*, 2013, 23, 731-738.
- [39] J. H. Waite, *Nat. Mater.*, 2008, 7, 8-9.
- [40] D. Shirley, *Phys. Rev. B*, 1972, 5, 4709-4714.
- [41] B. P. Tripathi, N. C. Dubey, S. Choudhury, F. Simon and M. Stamm, *J. Mater. Chem. B*, 2013, 1, 3397-3409.
- [42] B. P. Tripathi, N. C. Dubey, S. Choudhury and M. Stamm, *J. Mater. Chem.*, 2012, 22, 19981.
- [43] G. R. Guillen, T. P. Farrell, R. B. Kaner and E. M. V. Hoek, *J. Mater. Chem.*, 2010, 20, 4621.
- [44] S. J. Lue, C.-H. Chen, C.-M. Shih, M.-C. Tsai, C.-Y. Kuo and J.-Y. Lai, *J. Membr. Sci.*, 2011, 379, 330-340.
- [45] Q. Wang, S. Samitsu and I. Ichinose, *Adv. Mater.*, 2011, 23, 2004-2008.
- [46] A. M. Hollman and D. Bhattacharyya, *Langmuir*, 2004, 20, 5418-5424.
- [47] B. P. Tripathi, N. C. Dubey and M. Stamm, *J. Hazard. Mater.*, 2013, 252-253, 401-412.
- [48] D.-G. Kim, H. Kang, S. Han and J.-C. Lee, *J. Mater. Chem.*, 2012, 22, 8654.

- [49] M. Kumar and M. Ulbricht, *J. Membr. Sci.*, 2013, 448, 62-73.
- [50] W. Chen, Y. Su, J. Peng, X. Zhao, Z. Jiang, Y. Dong, Y. Zhang, Y. Liang and J. Liu, *Environ. Sci. Technol.*, 2011, 45, 6545-6552.
- [51] F. Bernsmann, A. Ponche, C. Ringwald, J. Hemmerlé, J. Raya, B. Bechinger, J.-C. Voegel, P. Schaaf and V. Ball, *J. Phys. Chem. C*, 2009, 113, 8234-8242.
- [52] D.T. Clark, A. Dilks: ESCA studies of polymers. XIII. Shake-up phenomena in substituted poly(styrenes). *J. Polymer Sci., Polymer Chem. Ed.*, 1977, 15, 15-30.
- [53] R. Yang and K. K. Gleason, *Langmuir*, 2012, 28, 12266-12274.
- [54] L. P. Zhu, J. H. Jiang, B. K. Zhu and Y. Y. Xu, *Colloids Surf. B Biointerfaces*, 2011, 86, 111-118.
- [55] C. Xue, N. Yonet-Tanyeri, N. Brouette, M. Sferrazza, P. V. Braun and D. E. Leckband, *Langmuir*, 2011, 27, 8810-8818.
- [56] Y. G. Takei, T. Aoki, K. Sanui, N. Ogata, Y. Sakurai and T. Okano, *Macromolecules*, 1994, 27, 6163-6166.
- [57] C. Veerman, L. M. C. Sagis, J. Heck and E. van der Linden, *Int. J. Biol. Macromol.*, 2003, 31, 139-146.

Table 1: Degree of immobilization (γ) of dopamine and PNIPAm, advancing (θ_{adv}) and receding (θ_{rec}) contact angle values, contact angle hysteresis ($\Delta\theta$), and solid-liquid free energy (ΔG_{sl}) of prepared membranes.

Membrane	γ [wt.-%]	θ_{adv} [°]	θ_{rec} [°]	$\Delta\theta$ [°]	$-\Delta G_{sl}$ [mJ·m ⁻²]
PET	00.00	56	23	33	113.49
PET-D	06.72	45	12	33	124.26
PET-N12	08.05	47	08	39	122.43
PET-N24	11.49	49	06	43	120.54

Table 2: Elemental surface composition of differently modified PET track-etched membranes.

The relative element ratios were determined from XPS wide-scan spectra.

Sample	[N]:[C]	[O]:[C]
PET	0.028	0.280
PET-D	0.071	0.238
PET-N24	0.098	0.216

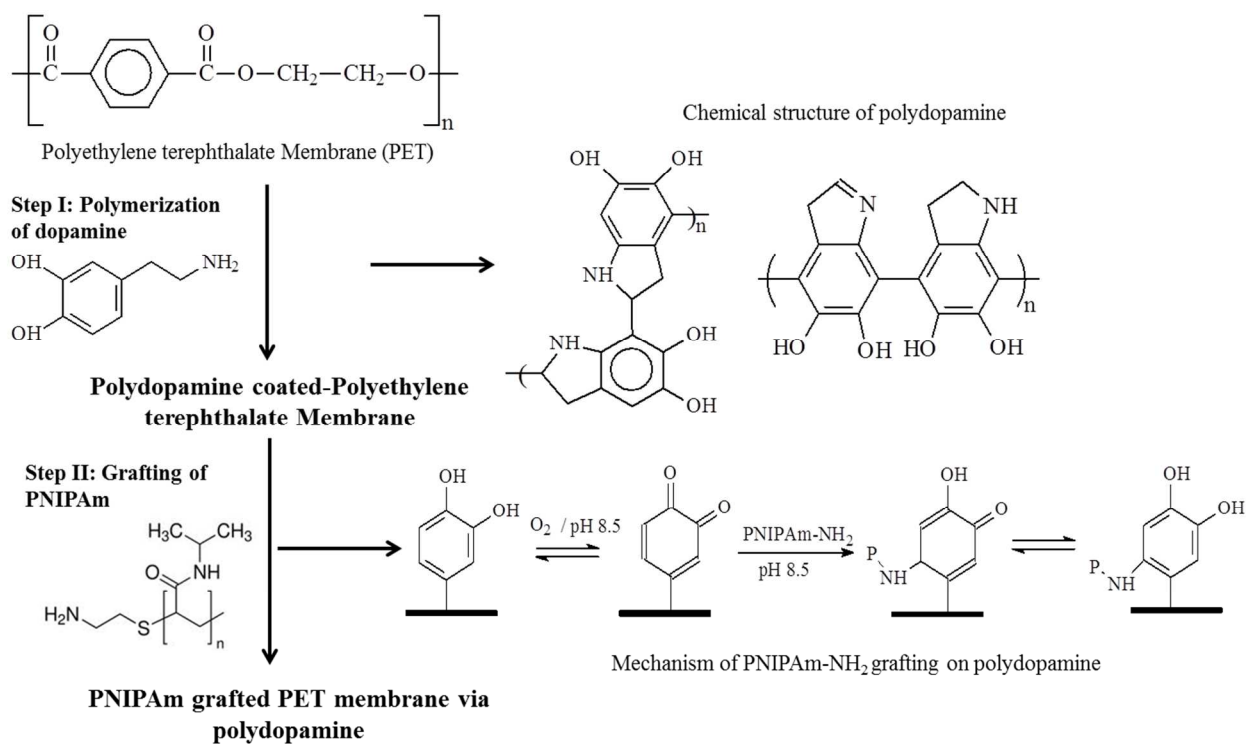


Fig. 1 Schematic route of membrane functionalization.

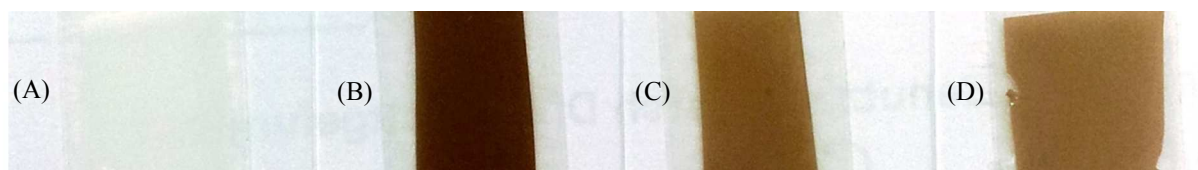


Fig. 2 Visual appearance of modified membranes: (A) PET; (B) PET-D; (C) PET-N12; and (D) PET-N24.

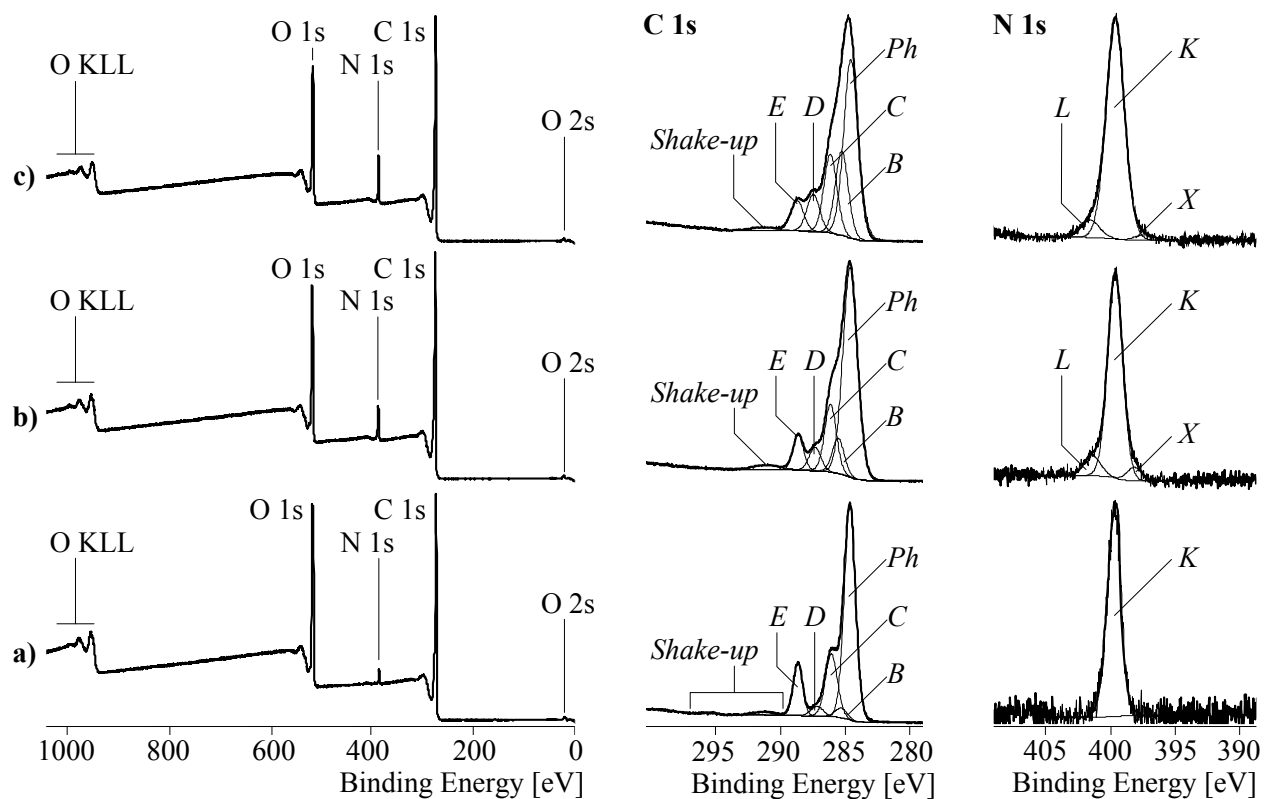


Fig. 3 Wide-scan XPS spectra (left column), C 1s (middle Column) and N 1s (right column) high-resolution XPS element spectra of a PET sample (a), a PET-D sample (b), and a PET-N24 sample (c).

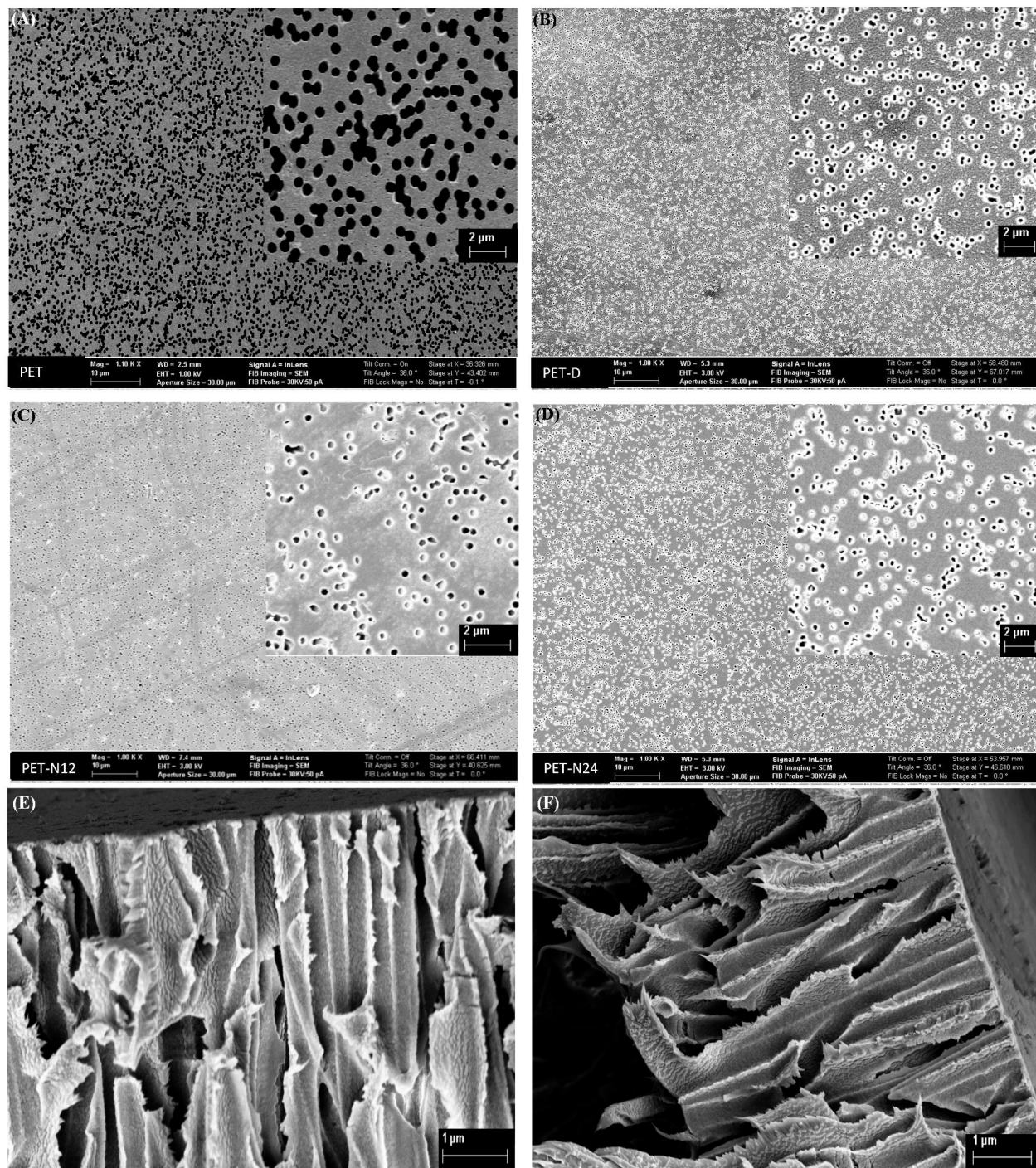


Fig. 4 Surface and cross-section SEM images of: (A) PET; (B) PET-D; (C) PET-N12; (D) PET-N24; (E) PET-D; and (F) PET-N24 membrane.

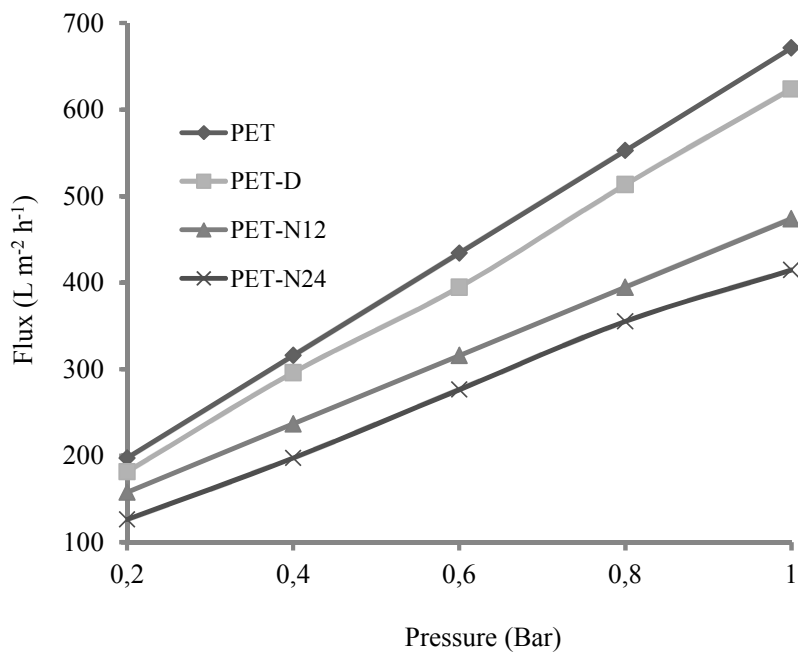


Fig. 5 Pure water flux vs. pressure variations.

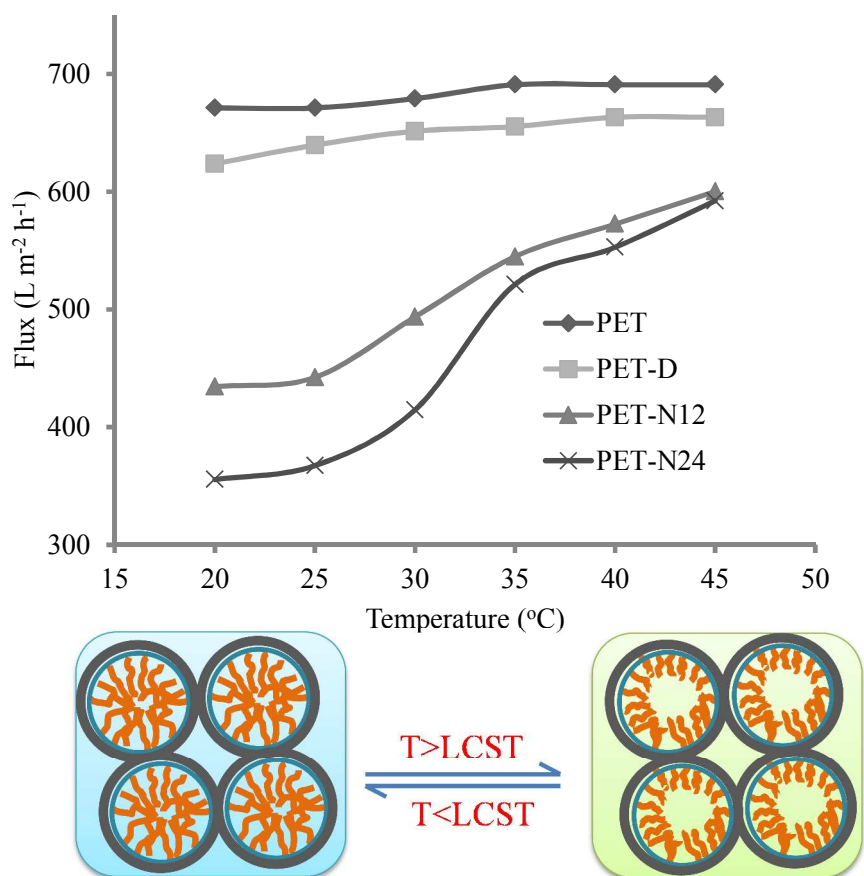


Fig. 6 Pure water flux vs. temperature variations and switching of pores above and below LCST.

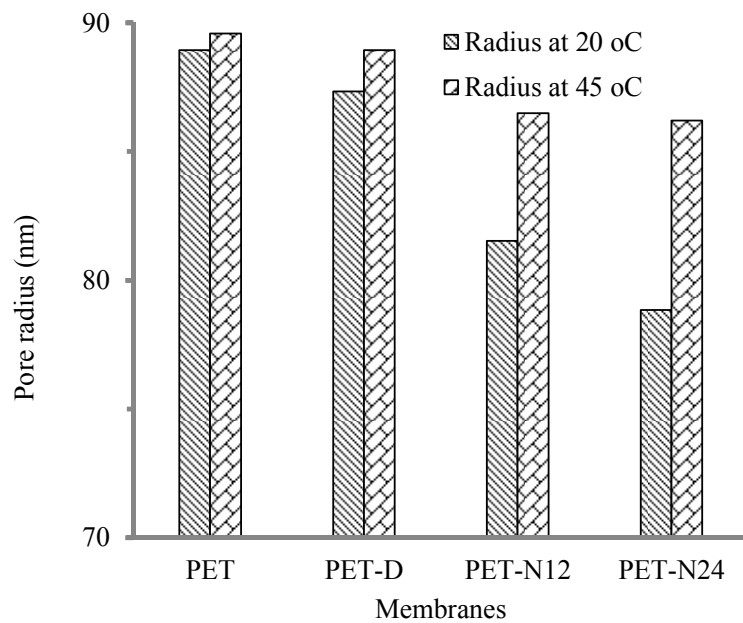


Fig. 7 Pore radius variation of membrane after the modification.

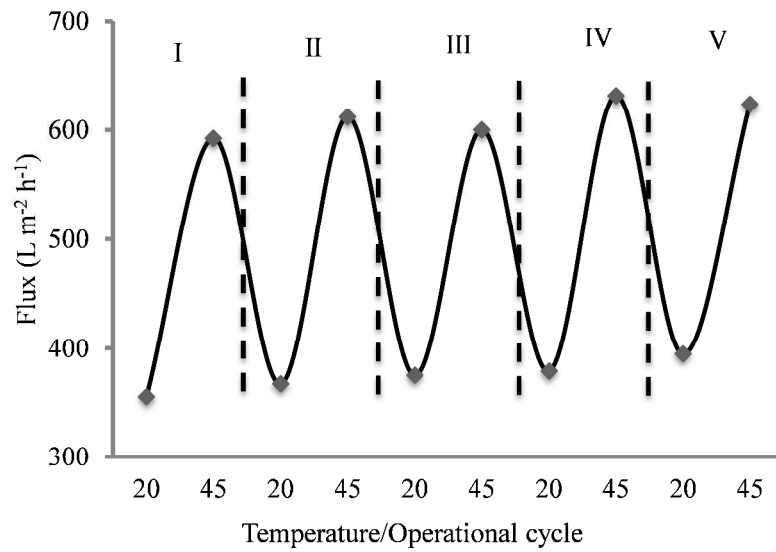


Fig. 8 Temperature response and operational stability of PET-N24 membrane.

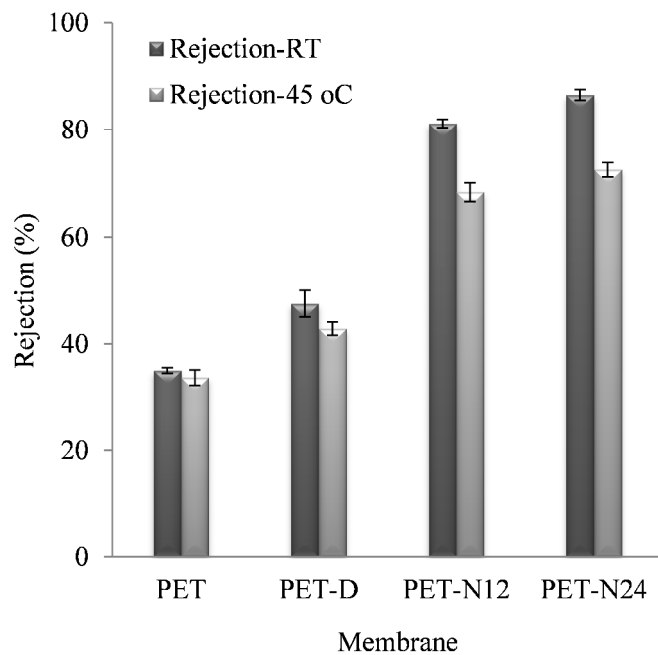


Fig. 9 BSA protein rejection performances of membranes.

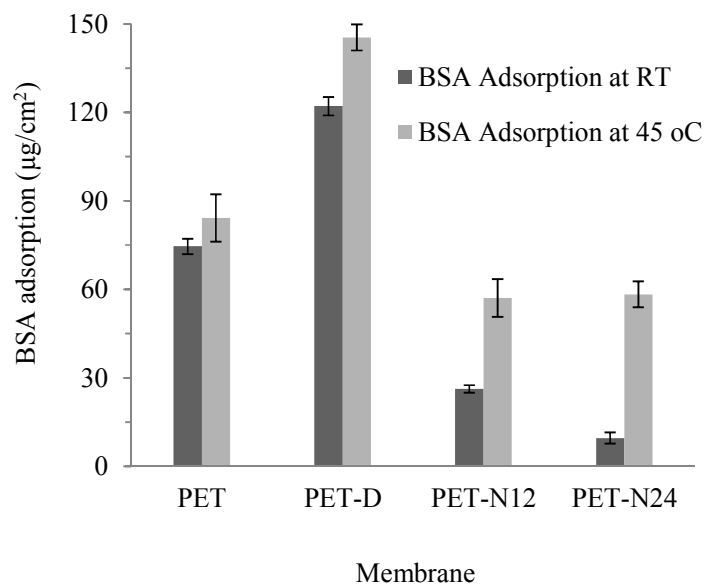


Fig. 10. Protein adsorption on membrane surfaces at room temperature and at 45 °C.

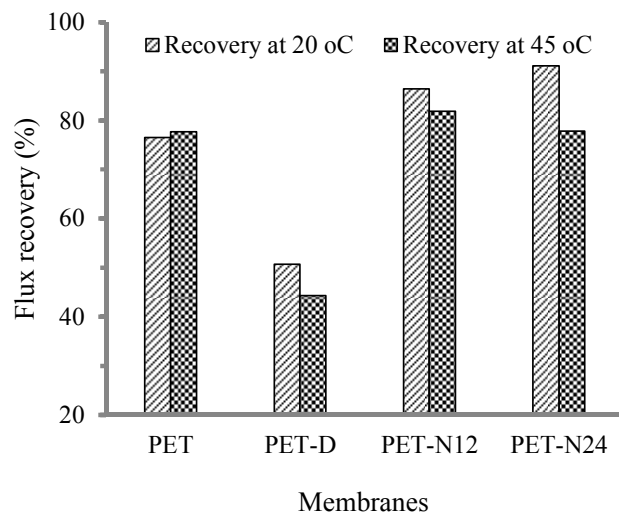


Fig. 11 Pure water flux recovery after fouling with BSA protein during ultrafiltration.

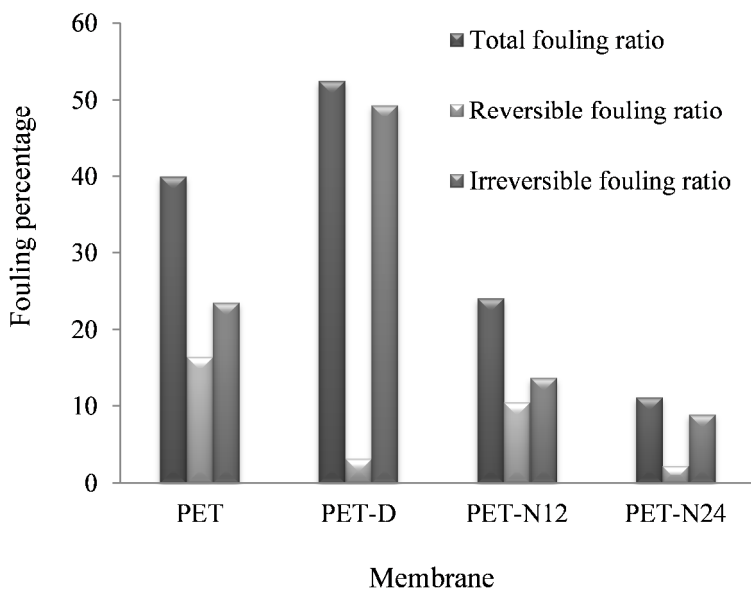


Fig. 12. The summary of the total fouling ratio (R_t), the reversible fouling ratio (R_r) and the irreversible fouling ratio (R_{ir}) for all prepared membranes.